Optical Changes in Unilamellar Vesicles Experiencing Osmotic Stress

G. White,* J. Pencer,* B. G. Nickel,* J. M. Wood,# and F. R. Hallett*
*Department of Physics and #Department of Microbiology, University of Guelph, Guelph, Ontario N1G 2W1 Canada

ABSTRACT Membrane properties that vary as a result of isotropic and transmembrane osmolality variations (osmotic stress) are of considerable relevance to mechanisms such as osmoregulation, in which a biological system "senses" and responds to changes in the osmotic environment. In this paper the light-scattering behavior of a model system consisting of large unilamellar vesicles of dioleoyl phosphatidyl glycerol (DOPG) is examined as a function of their osmotic environment. Osmotic downshifts lead to marked reductions in the scattered intensity, whereas osmotic upshifts lead to strong intensity increases. It is shown that these changes in the scattering intensity involve changes in the refractive index of the membrane bilayer that result from an alteration in the extent of hydration and/or the phospholipid packing density. By considering the energetics of osmotically stressed vesicles, and from explicit analysis of the Rayleigh-Gans-Debye scattering factors for spherical and ellipsoidal shells, we quantitatively demonstrate that although changes in vesicle volume and shape can arise in response to the imposition of osmotic stress, these factors alone cannot account for the observed changes in scattered intensity.

INTRODUCTION

Phospholipid membranes are permeable to water, small uncharged molecules (e.g., glycerol, urea), and small hydrophobic molecules but not to macromolecules or most hydrophilic species. Transporter proteins embedded in the cytoplasmic membranes of living cells mediate selective transmembrane fluxes of particular solutes, processes denoted as facilitated diffusion or active transport. In addition, proteinaceous channels may mediate more rapid and less selective transmembrane solute fluxes. Cells control their volume and/or turgor pressure by modulating cytoplasmic osmolality in response to changes in environmental osmolality. Such osmoregulation can be effected by transporters and channels that mediate the uptake or release of low-molecular-weight solutes that are otherwise compatible with cellular functions (Csonka and Hanson, 1991; Hallows and Knauf, 1994).

Milner et al. (1988) examined the behavior of osmoregulatory transporter ProP from bacterium *Escherichia coli*. ProP was activated when cytoplasmic membrane vesicles were subjected to an osmotic upshift with a membrane-impermeant solute (0.44 M sucrose or 0.30 M NaCl) but not with the membrane-permeant solute glycerol (0.30 M). The osmolality upshifts eliciting maximum activation of ProP in whole bacteria and cytoplasmic membrane vesicles are those imposed with 0.175 Osm kg^{-1} and 0.775 Osm kg^{-1} sucrose, respectively (Grothe et al., 1986; Marshall and Wood, unpublished data). Cytoplasmic membrane vesicles retain the size and topology of the cytoplasmic membrane, having radii in the range 550 to 700 nm, but they are devoid of both cell wall and cytoplasm (Altendorf and Staehelin, 1974).

Received for publication 21 June 1996 and in final form 16 August 1996.
Address reprint requests to Dr. F. Ross Hallett, Department of Physics, University of Guelph, Guelph, Ontario N1G 2W1 Canada. Tel.: 519-824-4120, X3989; Fax: 519-836-9967; E-mail: frh@physics.uoguelph.ca.

0006-3495/96/11/2701/15 $2.00

The observations of Milner et al. (1988) therefore suggested that ProP (or a membrane constituent with which it communicates) detects changes ensuing from osmotically activated transmembrane water flux, but not from changes in osmolality per se. Responses to changing transmembrane osmotic gradients (but not to osmolality itself) also characterize other osmoregulatory transporters (Csonka and Hanson, 1991).

To support further studies of ProP and of osmoregulation, we are developing methodologies for the detection and definition of membrane vesicle properties that change in response to the imposition of osmotic stress (Ertel et al., 1993; Hallett et al., 1993). Our previous research showed that 50-nm (radius) unilamellar DOPG (dioleoyl phosphatidyl glyerol) vesicles swell but do not rupture when they are diluted into hypotonic media and experience osmotic gradients up to approximately 0.5 osmol kg^{-1}. This maximum gradient corresponds to the "yield point" for leakage. The imposition of gradients larger than this elicits leakage of solutes from the vesicle lumen. Because this leakage serves only to return the osmotic gradient to the yield point value, such vesicles appear to remain swollen, with their membranes stretched (Ertel et al., 1993; Hallett et al., 1993). One question raised by that study was whether osmotically induced changes in the volume of phospholipid vesicles and in the lumenal concentration could be monitored by static laser light-scattering techniques. During the course of this investigation it became apparent that the scattering behavior of the membrane bilayer itself is strongly influenced by osmotic conditions. The results are consistent with the suggestion that changes in the medium osmolality elicit changes in the phospholipid packing and/or the hydration state of the bilayer. It is therefore possible that osmosensing, by integral or membrane-associated proteins, involves a response to these alterations in the bilayer environment.

In addition to the widespread use of membrane vesicles and reconstituted proteoliposomes as simple models of cell

membranes (e.g., Kaback, 1986), phospholipid vesicles are regularly used for the encapsulation of drugs, insecticides, and other chemical agents (Gregoriadis, 1984, 1995). Altered permeability of phospholipid vesicles to water and other species resulting from changing osmotic conditions is of considerable importance to these applications. Numerous determinations of passive transmembrane water flux can be found in the literature (Finkelstein, 1987; Jansen and Blume, 1995), and a number of mechanisms have been suggested to explain these observations (Kanchisa and Tsong, 1978; Deamer and Bramhall, 1986; Lawaczeck, 1988). Most of the observations are based on a light-scattering technique developed by Lawaczeck (1979, 1984, 1988) and Engelbert and Lawaczeck (1985) in which phospholipid vesicles, prepared in D_2O, are injected by a stop-flow apparatus into H_2O. The technique relies on the fact that the refractive index of D_2O differs slightly from that of H_2O. Immediately after injection the vesicles behave optically as coated spheres and demonstrate the corresponding scattering behavior. The opposing transmembrane fluxes of D_2O and H_2O lead to rapid equilibration, and the scattering decays to that characteristic of a hollow sphere. By monitoring the turbidity or the light scattered as a function of time after the injection, it is possible to determine the passive permeability of the vesicle membrane to water.

In other investigations this same approach has been used to study the osmotically driven water permeability of phospholipid vesicle membranes (Reeves and Dowben, 1970; Bittman and Blau, 1972; Carruthers and Melchior, 1983; Jansen and Blume, 1995). These cited studies relied on the differences in the refractive indices of the medium and the vesicle lumen, which arise from differences in their osmolyte concentrations. The observed changes in turbidity and scattering were attributed to the relative changes in these concentrations that arise from the transmembrane water flux and to the corresponding volume changes (swelling or shrinkage).

We show in this paper that phospholipid vesicle membranes exhibit surprisingly large optical changes in response to a changing osmotic environment. These changes are primarily attributed to changes in the refractive index of the bilayer arising from changes in the extent of membrane hydration and/or phospholipid packing. These changes are observed when small osmotic gradients (<200 mOsm kg^{-1}) are imposed or when vesicles are examined at different isotonic osmolalities. It is also demonstrated that changes in vesicle shape, arising from volume changes, cannot lead to the experimentally observed trends in scattered intensity. Variations in the optical properties of bilayers must, therefore, be considered when optical methods are used to determine vesicle membrane osmotic permeabilities, especially when performed at higher osmolalities. They must also be taken into account as further efforts are made to detect effects of transmembrane osmolality gradients on membrane structure and function.

THEORETICAL CONSIDERATIONS

The phospholipid vesicles used in this investigation are prepared by extrusion (see below), have an average radius of approximately 50 nm, are more than 95% unilamellar (Ertel et al., 1993), and have an estimated membrane thickness of 4.2 nm (Rutkowski et al., 1991). For particles of this size and wall thickness, the scattering factor (intraparticle structure factor) computed by Mie theory is essentially identical to that obtained by the Rayleigh-Gans-Debye (RGD) approach (Strawbridge and Hallett, 1994). Indeed, we will show below that under isotonic conditions, even the very simple Guinier approximation works well at scattering angles up to about 30° (for a light wavelength of 488 nm). Because the RGD and the Guinier formulas are much simpler functions, we have used them in the discussions that follow. However, we have used the Mie theory to confirm the results in selected "worst case" situations. The RGD scattering factor for a coated spherical particle is (Wyatt, 1973)

$$P(Q) = \left[(2R^3)(m_1 - 1)\left(\frac{j_1(u)}{u} + f^3\frac{(m_2 - m_1)}{(m_1 - 1)}\frac{j_1(u')}{u'}\right)\right]^2, \quad (1)$$

where j_1 is the first-order spherical Bessel function with argument, $u = QR$, or $u' = fQR$. Here R represents the outer radius of the vesicle, and Q represents the magnitude of the scattering vector, i.e.,

$$Q = \frac{4\pi n_0}{\lambda}\sin\left(\frac{\theta}{2}\right) \quad (2)$$

The incident light has a vacuum wavelength λ and is scattered at an angle θ from the through beam. The relative refractive indices are $m_1 = n_1/n_0$ and $m_2 = n_2/n_0$, where n_0, n_1, and n_2 are the refractive indices of the medium, the phospholipid bilayer, and the vesicle lumen, respectively (see Fig. 1).

The factor f in the Bessel function argument is related to the bilayer thickness t through the relation

$$f = 1 - \frac{t}{R}. \quad (3)$$

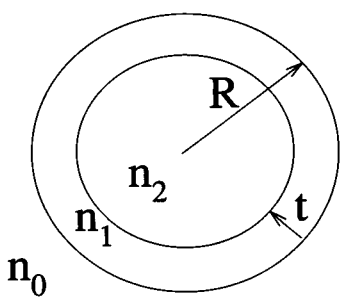

FIGURE 1 A schematic representation of a unilamellar vesicle. n_0, n_1, and n_2 are the indices of refraction of the medium, membrane and lumen, respectively. R is the outer radius of the vesicle and t is the bilayer thickness.

When initially extruded, the vesicles have a lumenal composition that is identical to that of the medium, in which case $m_2 = 1$ and Eq. 1 simplifies to

$$P(Q) = \left[(2R^3)(m_1 - 1)\left(\frac{j_1(u)}{u} - f^3\frac{j_1(u')}{u'}\right)\right]^2. \quad (4)$$

For the relatively thin-walled structures we are dealing with, Eq. 4 can be reduced to the simpler form

$$P(Q) = [2R_o^2 t_o(m_1 - 1)j_o(QR_o)]^2, \quad (5)$$

where $j_o(x) = \sin(x)/x$ is the zero-order Bessel function and R_o and t_o are an effective radius and thickness of the vesicle bilayer. In particular, Eqs. 4 and 5 are identical for small scattering angles (small Q) if we identify R_o as the radius of gyration of the bilayerand 4 $\pi R_o^2 t_o$ as the bilayer volume, i.e.,

$$R_0^2 = \frac{3R^2}{5}\frac{(1 - f^5)}{(1 - f^3)}, \quad R_0^2 t_0 = \frac{R_0^3}{3}(1 - f^3). \quad (6)$$

The Guinier expression (Tanford, 1961) for a spherical thin shell,

$$P(Q) = [2R_o^2 t_o(m_1 - 1)]^2(1 - Q^2R_o^2/3) \quad (7)$$

can be derived from the expansion of j_o in Eq. 5 and is valid in our case for scattering angles of less than about 30°.

In the following sections we will discuss changes in both the magnitude and Q dependence of the measured scattered intensity,

$$I(Q) \approx k^4P(Q) = \left(\frac{2\pi n_0}{\lambda}\right)^4 P(Q) \quad (8)$$

as the osmolality of the medium is either decreased so as to produce a hypoosmotic shift and vesicle swelling, or increased, so as to produce a hyperosmotic shift and shrinkage. If, for example, an osmolality gradient is established across the membrane by dilution of the extravesicular medium to produce hypoosmotic swelling, then the angle dependence of the scattered intensity evolves from that of a hollow sphere (Eq. 4) to that of a coated sphere (Eq. 1). The magnitude of the scattering can change with the concentration of the medium due to changes in n_0 and sometimes n_2, and if small changes in intensity are to be interpreted properly, the values of n_0, n_1, and n_2 must be accurately known at the wavelength of the incident light and at each concentration of the medium. Explicit attention to n_0, n_1, and n_2 distinguishes the current study from studies that have been based on 1) the assumption that vesicles behave as ideal osmometers, and 2) the assumption that the refractive index of the membrane, n_1, is constant at all osmolalities and osmotic gradients (e.g., Bittman and Blau, 1972; Jansen and Blume, 1995; Lawaczeck, 1984).

The possibility also exists that alterations in the vesicular shape, caused by changes in the osmolality of the medium, could influence scattering behavior. For example, during an osmotic upshift of the extravesicular medium, the vesicle could increase its eccentricity (become more ellipsoidal) as it seeks to reduce the lumenal volume. We deal with this question at some length in Appendix B and show that shape changes (at constant surface area) cannot account for the observed trends in scattered intensity. We will conclude that we cannot account for these trends unless the refractive index of the membrane n_1 is permitted to vary during osmotic swelling and shrinking of the vesicle.

EXPERIMENTAL PROCEDURES

In all cases large unilamellar vesicles (LUVs) of DOPG were prepared in the manner outlined by Ertel et al. (1993) and Mayer et al. (1985). DOPG (Avanti Polar Lipids, Alabaster, AL) in powder form was dissolved in dichloromethane (Fisher Scientific Co., Mississauga, ON), and the solvent was then removed by rotary evaporation followed by drying under vacuum (vacuum pump model 24; Precision Scientific Co., Chicago, IL) for 10 min in a vacuum dessicator with no dessicant. The dried lipid film was then dispersed (by stirring for 30 min) into a medium buffered with 20 mM NaMOPS (NaMOPS is the sodium salt of morpholinopropane sulfonic acid), adjusted to pH 7.4 using NaOH, and containing the amount of NaCl needed to achieve the desired total osmolality (usually about 1550 mOsm kg^{-1}). The concentration of this preliminary dispersion of DOPG multilamellar vesicles was 50 mg lipid/ml medium. This mixture was then frozen and thawed 10 times by cycling it through liquid nitrogen and a warm water bath before extrusion in a stainless steel device similar to that described by Nayar et al. (1989). In this device LUVs were created by forcing the dispersion through a single 25-mm (diameter) Nucleopore polycarbonate filter (50-nm pore radius) using compressed N_2 gas at a pressure of 100–300 lb in^{-2}. A water-filled jacket surrounded the extruder and maintained a constant temperature of 25°C, ensuring that the DOPG was in the liquid crystal phase during extrusion. The extrusion was repeated 10 times for each preparation. The resulting LUVs were over 95% unilamellar (Ertel et al., 1993) and were narrowly distributed about a mean radius of approximately 50 nm, as determined by dynamic light scattering. The osmolalities of the buffered media used for the vesicle studies were determined experimentally with a vapor pressure osmometer (Wescor, Logan, UT).

For static light-scattering purposes, the LUV preparations were diluted to yield a final concentration of 0.02–0.05 mg DOPG/ml with medium that was made hypotonic, isotonic, or hypertonic (with respect to the medium employed during extrusion) by varying the NaCl concentration. The final vesicle concentration and the concentration of the MOPS buffer were identical in every experiment. The swelling or shrinkage experiments were performed by the addition of hypotonic or hypertonic media to obtain the required osmolality downshifts or upshifts.

The static light-scattering experiments were performed using a fiber optic-based light-scattering instrument described previously (Strawbridge and Hallett, 1992). The light source was an argon laser (Lexel model 95; Lexel Laser, Fremont, CA) operating at 488 nm. The apparatus allowed the measurement of scattered intensities at 20 scattering angles ranging from 16° to 160°. The light scattered from a cylindrical sample cell passed through a surrounding water bath (maintained at 25°C) into a set of collimating slits that served to define each scattering angle to ±0.1°. The light at each angle was directed via the fiber optic cables to a single photomultiplier (PMT model RFI/B263F; Thorn EMI, Hayes, England). The photomultiplier signal was amplified, discriminated, and converted to TTL pulses by a photon counter (Stanford Research Systems SR440, Stanford, CA). Background measurements were taken on solutions of pure water or buffered media. Calibration of the instrument was performed using 96-nm-diameter latex spheres (Duke Scientific Corp., Palo Alto, CA). A shutter under computer (IBM-PC compatible) control allowed each fiber optic to be selected in turn and the data collection interval to be varied. The final intensity measurements for each scattering angle were obtained as digital counts that could be stored on disk for subsequent analysis. The measurement of the angular dependence of the scattered light

intensity also allows, through a discrete Laplace inversion, simultaneous determination of vesicle size distributions (Strawbridge and Hallett, 1994). These determinations are essential if the changes in scattered intensity are to be attributed to optical changes in the membrane and not to vesicle aggregation. This procedure, as well as theoretical predictions of scattering intensity changes, requires knowledge of the refractive indices of the media at all concentrations and at a wavelength of 488 nm. These refractive index measurements were conducted on a precision goniometer, using the angle of minimum deviation method (Freeman, 1990).

The refractive index n_o and the osmolality of the extravesicular medium were measured as the NaCl concentration of the medium was varied. Fig. 2 provides a plot of the refractive index versus osmolality for a wavelength of 488 nm, which is the wavelength of the laser source. Regression analysis of this data ($r^2 = 0.993$) yielded the relationship

$$n_0(c) = 1.3378 + 5.5142 \times 10^{-6}c, \quad (9)$$

where c is the osmolality of the medium in mOsm kg^{-1}.

For independent verification of the changes in scattered light intensity caused by osmolality changes, turbidity was measured using a UV-visible spectrophotometer (Beckman DU-65; Beckman Instruments, Fullerton, CA). The results were consistent with those described earlier (Bangham et al., 1967) and have not been reproduced here.

RESULTS AND DISCUSSION

Previously (Ertel et al., 1993; Hallett et al., 1993) we were able to show that with increasing dilution into a hypotonic medium, unilamellar DOPG vesicles first exhibited a gradual swelling phase, followed by a leakage phase at osmolality gradients greater than approximately 500 mOsm kg^{-1}. In the studies reported here we are only concerned with the scattering changes associated with relatively small (<200 mOsm kg^{-1}) changes in osmolality from the isotonic case and the relatively small swelling/shrinkage effects that they induce. The use of these relatively small gradients ensures that our observations relate to changes in membrane properties induced by osmotic gradients, with no added complexity of changes due to solute leakage effects. Gradients in this range are sensed during osmoadaptation by living cells.

The angle dependence of the intensity of light, $I(Q)$, scattered by the DOPG vesicles in isotonic medium (1550 mOsm kg^{-1}) is shown in Fig. 3. By using a discrete Laplace inversion routine (Strawbridge and Hallett, 1994), the corresponding size distribution of the vesicles was recovered from $I(Q)$, and typical results (both number and intensity-weighted distributions) are shown in Fig. 4. These distributions were found to be highly reproducible, with mean sizes of different preparations varying by only 1–2 nm from a number average radius of 51 nm. This size is consistent with the use of filters with a pore radius of 50 nm in the extruder. The intensity average size of the vesicles was 69 ± 2 nm.

Calculation of expected scattered intensities

The expected intensity of light scattered by such vesicles after the dilution or concentration of the extravesicular medium (osmotic down- or upshift) was computed by using Eqs. 1–8. These equations require values for n_0, n_1, n_2, R, and t. For DOPG vesicles suspended in isotonic medium, the value of t was taken to be 4.2 nm (Rutkowski et al., 1991). Because the total mass of membrane must remain constant during shrinkage or swelling, it was assumed that

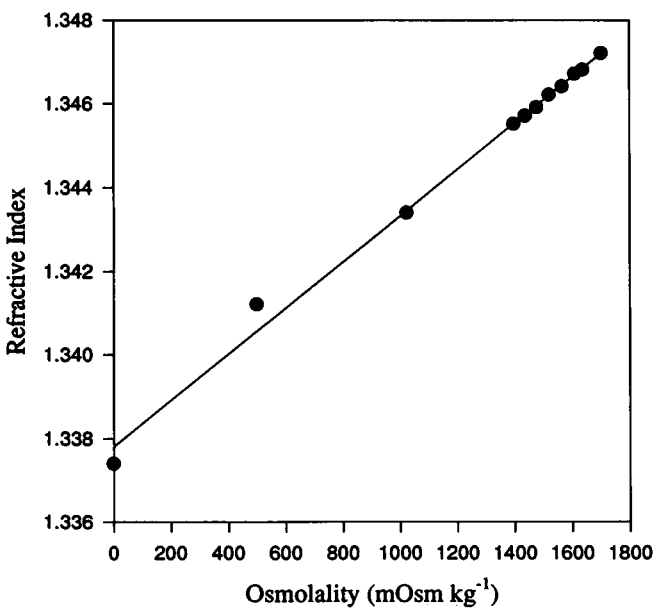

FIGURE 2 Measured refractive index of the NaMOPS-NaCl medium (n_0) as a function of osmolality (obtained by adjusting the NaCl concentration). In the given range, the medium refractive index varies linearly with osmolality, and the fit function (*solid line*) is given as Eq. 9.

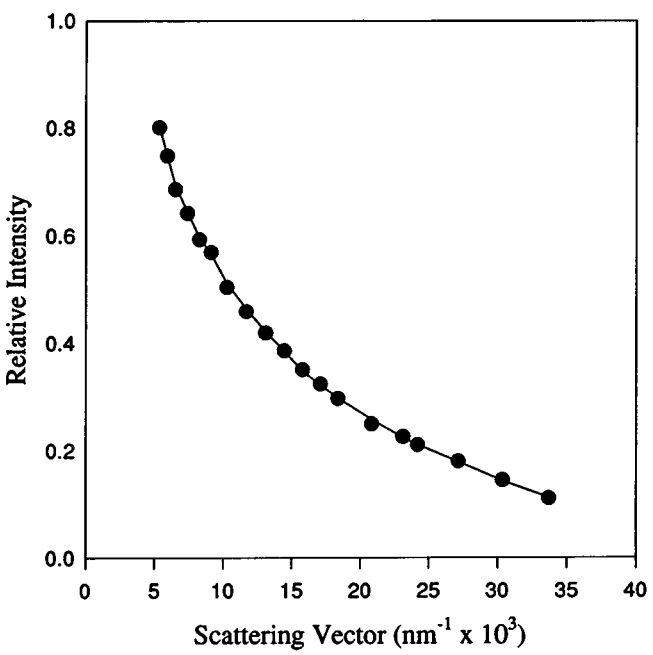

FIGURE 3 Relative scattered intensity from DOPG vesicles in an isotonic medium as a function of scattering vector **Q**. The points correspond to experimental data, and the solid line corresponds to a fit obtained by discrete inversion of the data, yielding the size distributions shown in Fig. 4.

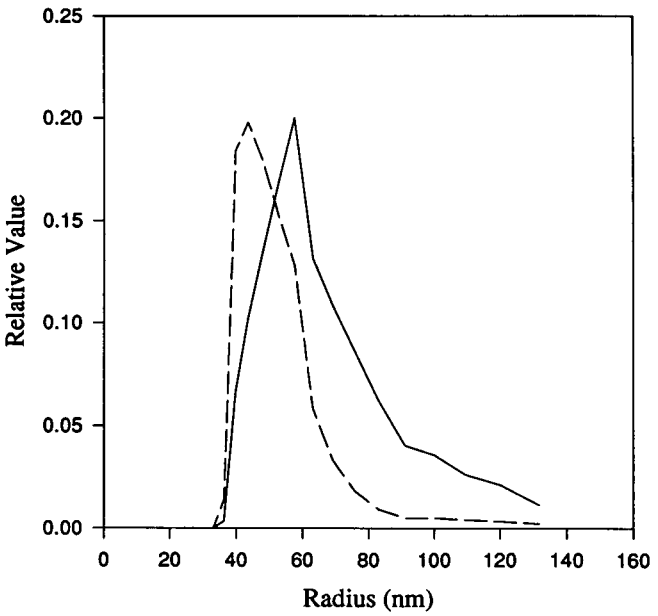

FIGURE 4 The number distribution (*dashed line*) and the intensity distribution (*solid line*) of vesicle radii determined using a discrete Laplace inversion of the experimentally determined scattering results of Fig. 3.

the membrane volume remained constant as well. This required slight thinning during swelling and a slight thickening during shrinkage. These corrections to t, although very small, were included in the calculations.

The value of the refractive index of the extravesicular medium n_0 was the experimentally measured value corresponding to each osmolality (see Fig. 2). For the other parameters a choice or computation was made that can be described as follows. It was first assumed that the refractive index of the membrane, n_1, was constant and independent of the concentration of the extravesicular medium. This is the common assumption of Jansen and Blume (1995), Lawaczeck (1984), and others (see Introduction). We have used a value of 1.458 (Sober, 1968) for the average refractive index of the membrane, n_1. This value is a compromise in that it represents the refractive index of oleic acid at 589 nm. One would expect the refractive index to be slightly higher than this at 488 nm, the wavelength of our laser source. However, the headgroup region of the membrane is thought to have a refractive index somewhat lower than that of the acyl chain region. As a result, the value chosen may be fairly realistic. Regardless of the value chosen, however, the qualitative observations that are made in the following sections remain intact.

For the two remaining parameters n_2 and R, one must treat separately the case of osmotic downshift and upshift. For the former one can assume the vesicle remains spherical but swells slightly as a result of the osmolality gradient. The degree of swelling depends on the area compressibility of the vesicle membrane. The elementary calculation of Hallett et al. (1993) is repeated in Appendix A, with the result that the internal concentration c_{int} partly tracks the extravesicular concentration c_{ext}, as this is lowered from the isotonic value c_{iso}. The tracking also depends on vesicle radius and, for our vesicle size range, we use the relationship

$$(c_{int} - c_{ext}) \approx (0.5 \text{ to } 0.7)(c_{iso} - c_{ext}), \qquad (10)$$

where the value spread in the coefficient of proportionality is based on the spread of literature values for the membrane area compressibility (Hallett et al., 1993; Niggemann et al., 1995). Given c_{int} from Eq. 10 we determine n_2 using the measurements summarized in Eq. 9. Finally, we determine the vesicle radius R from the inverse proportionality of the lumen volume to the lumen concentration and from the isotonic value $R_0 \approx 70$ nm that represents the intensity-averaged radius as determined from the discrete Laplace inversion of $I(Q)$ (see Fig. 4).

In the case of osmotic upshift the concentration gradients are such as to tend to reduce the lumen volume (by outward water flow), and the vesicle can accommodate such reduction by changing shape. There is little change in membrane area, and the shape change is resisted predominantly by curvature energy in the membrane, as discussed in some detail in Appendix A. There we also conclude that the curvature energy is too small to support any significant concentration gradient, and we can take $c_{int} = c_{ext}$ and hence $n_2 = n_0$ with negligible error. The precise shape of the minimum energy vesicle can only be determined numerically (Jenkins, 1977; Seifert et al., 1991), but for volume changes of less than about 25% that occur here, the approximation of the shape to a prolate ellipsoid of revolution is entirely adequate for purposes of estimating light-scattering intensities. This is because the combination of small vesicle size and low scattering angle implies that all parts of the vesicle membrane contribute equally to the scattered electric field amplitude, with the result that the intensity is independent of anything but very gross structural changes. The most important indicator of these changes is the radius of gyration, and explicit calculation shows that the radius of gyration of a prolate ellipsoid differs from that of the exact surface enclosing the same volume by less than 0.5%, this again for volume reduction factors of less than 25%. We have further confirmed this assertion of structural independence by showing that even the very crude approximation of leaving the vesicle as a spherical shell of fixed radius R_0 still gives nearly the same angular dependence and total intensity of the scattered light.

The details of the prolate ellipsoid calculation are described in Appendix B. In essence we model the vesicle as a thin membrane with semimajor and semiminor axes a and b. We take $c_{int} = c_{ext}$ and $n_2 = n_0$ as above and fix the surface area of the ellipsoid to the original sphere area $4\pi R_0^2$. The thickness t_0 is also left unchanged, so that the membrane volume responsible for the scattering is unchanged. Finally, from the scaling relation lumen volume $\propto 1/c_{int}$, we can determine the required axes parameters. At 10% lumen volume reduction, the axial ratio $a/b \approx 2.0$; at 25% reduction the ratio has increased to $a/b \approx 3.3$. These

relatively large changes in shape do not imply a corresponding large change in the light-scattering intensity because even for the 25% volume reduction case the radius of gyration has only increased by 16%, as shown in Fig. 12. Combining this last result with the Guinier scattering factor $1 - Q^2R_g^2/3$ for an arbitrary shape (Tanford, 1961) implies a mere 2.5% reduction in the intensity for an average sphere radius of ~70 nm and scattering at 22°. (In principle there could be a change in the scattering intensity due to what are known as depolarization effects that can arise when a vesicle changes shape. We have estimated what changes might occur for the hollow ellipsoids representing the vesicles and believe that in all cases the effects on the scattered light intensity are much less than 1% and are negligible relative to the other calculated effects and observed changes (see Appendix B).)

Thus size and shape changes are predicted to have relatively little influence on the scattered light intensity. The effects that are seen must arise out of changes in scattering power and/or optical contrast between the bilayer, the lumen, and the extravesicular medium. To simplify the qualitative discussion of this point, assume that $Q \approx 0$ (for small scattering angles) and near-isotonic conditions. In that case one can show from Eqs. 1 and 8 that the relative intensity change is related to index of refraction changes by

$$\frac{\delta I}{I} = 4\frac{\delta n_0}{n_0} + \frac{2}{m_1 - 1}\left(\delta m_1 + \frac{f^3}{1 - f^3}\delta m_2\right). \quad (11)$$

The different terms in Eq. 11 can be simply interpreted to yield the relative contribution of each source of change. The δn_o term arises out of the prefactor in Eq. 8 and is the result of the enhancement of the radiation of a dipole embedded in a medium with $n_o > 1$. The δm_1 and δm_2 terms are the result of the change in optical contrast between the external medium and the vesicle membrane and lumen, respectively. The prefactor of δm_2 accounts for the relatively larger volume of the lumen relative to the membrane, and for our vesicles of (intensity average) radius 69 nm and membrane thickness ~4.2 nm this factor is $f^3/(1 - f^3) \approx 4.8$.

Equation 11 can be used to investigate a number of simplifying assumptions. The crudest, and one that is certainly not realistic, is that only the external medium index n_o changes, in which case $\delta m_1 = -m_1\delta n_o/n_o$ and $\delta m_2 = -\delta n_o/n_o$. Then the change in intensity becomes

$$\frac{\delta I}{I} = \left[4 - \frac{2m_1}{m_1 - 1} - \frac{2f^3}{(m_1 - 1)(1 - f^3)}\right]\frac{\delta n_0}{n_0}, \quad (12)$$

and the numerical values of the three terms in [ ] corresponding to scattering power and bilayer and lumen contrast, respectively, are 4, ≃26, and ≃116. Clearly in this approximation the lumen plays the most important role. The combined result $\delta I/I \approx -138\delta n_o/n_o$, in conjunction with the index measurement in Eq. 9, predicts an 14% decrease in intensity for each 250-mOsm kg^{-1} upshift in concentration in the external medium and a corresponding 14% increase in scattering for the same reduction in concentration. As we have argued above, the internal medium concentration will also change, with the result that δm_2 will not be as large. Thus Eq. 12 represents a limit to the predicted changes. Fig. 5 shows what is expected from this limiting approximation for finite Q; that is, for this figure we have assumed that the vesicle is perfectly rigid so as to maintain an unchanged internal volume and concentration.

A more realistic treatment incorporates the elastic (deformable) properties of vesicles. First let us consider the effects of osmotic downshift. We can use Eq. 10 for the change in internal medium concentration and find $\delta m_2 \approx -(0.5 \text{ to } 0.7)\delta n_o/n_o$, which is to say that the lumen contrast is now reduced from what it would have been for a rigid spherical vesicle. The change in scattering intensity from Eq. 11 now is in the range $\delta I/I \approx -(80 \text{ to } 103)\delta n_o/n_o$, but it is still the case that the dominant contribution is from the lumen contrast. These results for $Q \approx 0$ remain qualitatively valid for finite Q and are shown in Fig. 6 as the set of lines marked (b). For the osmotic downshift region, where the vesicle remains spherical, these calculations are based on Eqs. 1–8. For comparison purposes, the rigid sphere results (from Fig. 5) at low Q are also shown as the set of lines marked (a).

For the osmotic upshift we have used the more accurate equations in Appendix B that allow for the vesicle shape changes to prolate ellipsoids (see Fig. 6, lines (c)). For osmotic upshift conditions, internal and external concentrations (and refractive indices) remain identical, so that now $\delta m_2 = 0$ and $\delta I/I \approx -22\delta n_o/n_o$. The relatively small size of this $\delta I/I$ simply reflects the fact that the vesicle bilayer is not a large scattering volume. Because we show only relative intensities, very little dependence on angle is expected. The

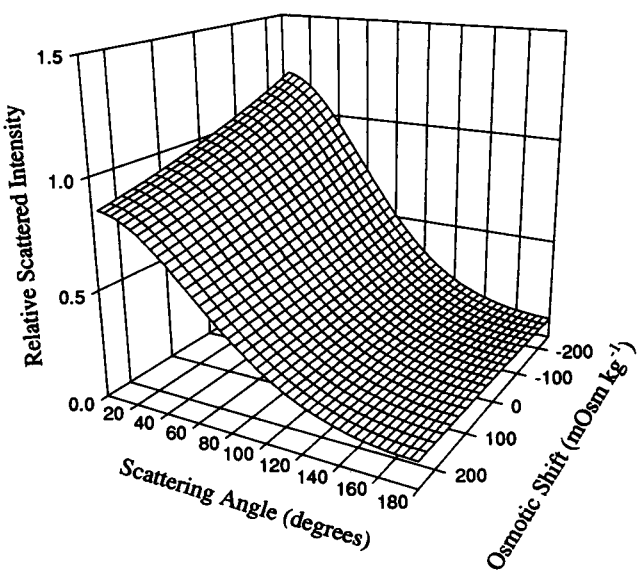

FIGURE 5 Theoretically predicted relative scattered intensity as a function of scattering angle and medium osmolality. This initial calculation uses the assumptions that vesicles are rigid structures and that the refractive index of the bilayer is constant.

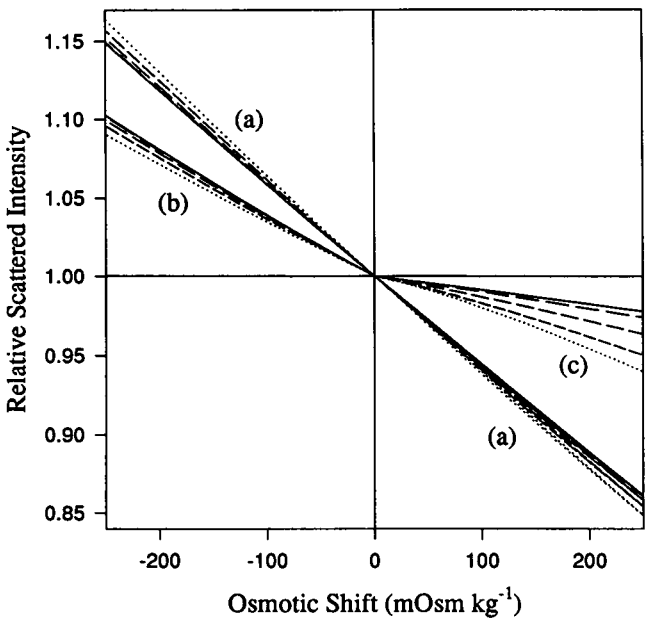

FIGURE 6 Theoretically predicted relative scattered intensity versus the difference between medium osmolality and its isotonic value for rigid spherical shells (*lines a* as from Fig. 5), for elastic spherical shells (*lines b*) undergoing increasing strain with increasing osmotic downshift, and ellipsoidal shells (*lines c*) that exhibit decreasing volume with increasing osmotic upshift. Again, for all cases the refractive index of the bilayer is held constant. The solid lines represent the intensities at 0° scattering angle. The dashed to dotted lines represent intensities at scattering angles of 15°, 30°, 45°, and 60°.

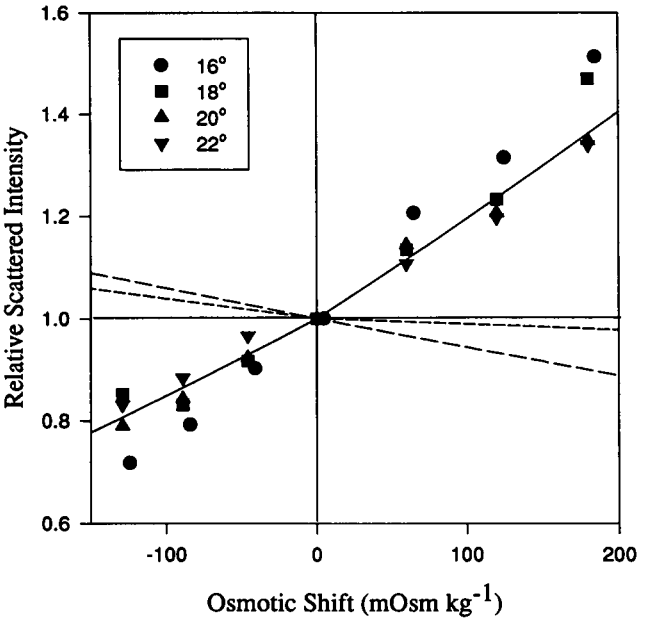

FIGURE 7 The symbols correspond to the experimentally determined scattering curves at the scattering angles shown in the figure as a function of osmotic upshift or downshift due to changes in the NaCl concentration of the medium. The samples were prepared with a medium osmolality of 1550 mOsm kg^{-1}; the final osmolalities of the suspending media differed from this value by (in order of osmotic shift) −129, −89, −46, 0, +60, +120, +180 mOsm kg^{-1}. The dashed lines are the theoretically predicted intensities as in Fig. 6 for rigid spherical shells (*long dash*), elastic spherical shells, and ellipsoidal shells (*short dash*) for a scattering angle of 20°. Notice that the experimental results and these theoretical predictions differ in both magnitude and sign. The solid line through the data is not a fit, but is a theoretical simulation (see text) of the scattering behavior of vesicles at 20° scattering angle that is similar to the elastic shell/ellipsoid computation (*short dashed line*), but where the refractive index of the bilayer n_1 is allowed to vary linearly with external osmolality, as in Fig. 8.

(very weak) angle dependence that remains in the case of osmotic downshift is, in part, the result of vesicle expansion and, in part, of the cross-over from shell scattering to volume scattering as the external medium concentration is changed and optical contrast with the lumen develops. For upshift conditions it is the changing shape and radius of gyration of the vesicle that lead to the observed angle dependence.

Note that the qualitative feature of intensity increase with osmotic downshift and intensity decrease with upshift cannot be changed by small changes in any of the parameters of a model that assumes a constant bilayer refractive index n_1. We return to this important point after the discussion of our experimentally observed intensity changes.

Observed changes in scattered intensities

The measured values of $I(Q)$, relative to the isotonic case, for the range of osmotic shifts used in the model calculations above are shown as symbols in Fig. 7. Also included in this figure (*dashed lines*) are the predicted results for a 20° scattering angle (calculated as in Fig. 6, *lines* (*b*) and (*c*)). It is immediately obvious that the measured trend is both much larger than and in the opposite direction to the predicted results shown in Figs. 5 and 6. Changes similar to this have been observed in turbidity measurements on large unilamellar vesicles (Bangham et al., 1967; Abuin et al., 1995) and in the scattering from preparations of multilamellar vesicles (Yoshikawa et al., 1983). At the largest osmotic downshift shown, the intensity change at a scattering angle of 16° approaches a 30% decrease from the isotonic value, whereas the computed prediction would suggest a 10% increase.

It is possible that the changes in intensity are somehow connected to a change in the aggregation state of the vesicles. However, neither the original isotonic particle size distribution nor that after an osmotic shift provides any indication of aggregation. Using NNLS exponential sampling analysis of dynamic light scattering data (Hallett et al., 1989, 1991) and/or discrete Laplace inversion of the measured $I(Q)$ data (Strawbridge and Hallett, 1994), we observe small linear increases (up to a few percent) in effective particle size with increasing osmotic downshift and small decreases in particle size with osmotic upshift. We hesitate to interpret these latter size changes quantitatively because, as opposed to the isotonic case, the recovery of number distributions with either scattering method requires, for example, accurate estimates of n_1 and n_2 at each osmotic shift.

A second possibility is that the intensity changes that are observed result from changes in vesicle shape. The detailed calculations in Appendix B and summarized in Fig. 6, *line (c)*, show that significant intensity changes are not expected from vesicles that begin as spheres under isotonic conditions and change under osmotic upshift into the prolate objects determined by the bilayer curvature energy given in Eq. A1. We have no independent evidence of the actual shapes adopted by vesicles under our experimental conditions. However, our vesicles are small relative to the wavelength of the light source, and it is hard to imagine any reasonable shape changes that could account for anything more than a few percent change in scattering intensity. Thus our conclusion that changes in shape cannot account for the observed experimental trends in Fig. 7 is quite independent of the particular model building described in Appendices A and B.

Because aggregation and shape changes can be discounted, the observed trend in scattering intensity must arise from changes in the optical/structural properties of the vesicle membrane bilayer. Either the thickness or the refractive index of the bilayer must be altered in response to the osmotic environment. However, multilamellar membranes have been studied under a variety of osmotic conditions (Rand and Parsegian, 1989), and there is no indication of large changes in the bilayer thickness. This leaves the membrane refractive index n_1 as the most likely parameter responsible. The solid line in Fig. 7 is a simulation that matches the observed scattering changes that occur during osmotic shift, but where n_1 is allowed to change linearly with the concentration of the extravesicular medium. To achieve this match, the value of n_1 would have to increase linearly from a value of 1.442 at a maximum downshift of -150 mOsm kg^{-1} to 1.480 at a maximum upshift of 200 mOsm kg^{-1} (see Fig. 8). This corresponds to a remarkable change in refractive index (0.039) over a total osmolality change of ~350 mOsm kg^{-1}.

The lowering of n_1 in response to increasing the osmotic downshift of the extravesicular medium could arise from the developing membrane strain, changes in the extent of membrane hydration, or some combination of the two. A reduction in the phospholipid packing density could accompany either. Although the imposition of membrane strain could contribute to the reduction in n_1 in the osmotic downshift experiments, it is unlikely that strain could play a significant role during upshift, because the membrane should be in an unstrained condition at all osmolalities above the isotonic value (see Appendix A). This suggests that hydration is primarily responsible for the changes in n_1. To confirm this, scattered intensities were obtained from vesicles extruded under identical conditions in media with osmolalities of 500, 1000, and 1500 mOsm kg^{-1}. Under isotonic conditions the vesicles in each medium should all be in a similar unswollen state. However, Fig. 9 indicates that dramatic differences in scattering intensity are present and that the scattered intensity increases dramatically with increasing osmolality of the medium, even though the vesicle size

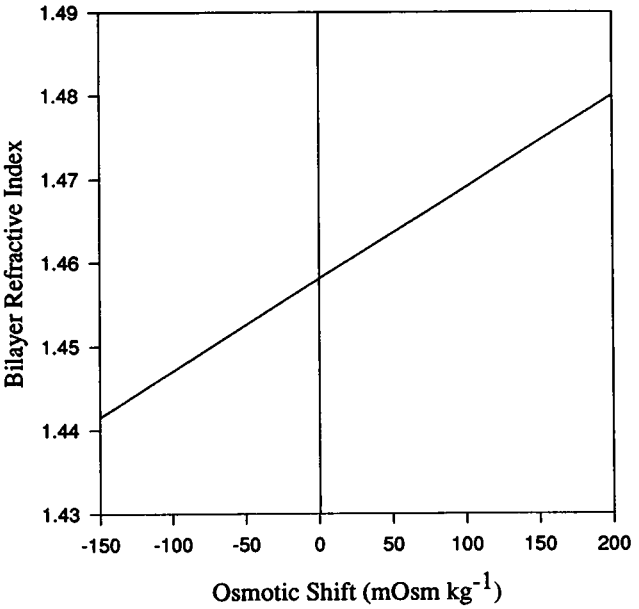

FIGURE 8 Variation of the bilayer refractive index (n_1) plotted as a function of the osmotic shift. This linear variation is required to match the experimental results in Fig. 7 and can be described by the equation $n_1 = 1.458 + 11.0 \times 10^{-5}\ \Delta C$, where ΔC is the osmotic shift (mOsm kg^{-1}).

distributions in all three preparations are very similar (see inset to Fig. 9). These results suggest that membrane hydration is the principal factor that contributes to the changing optical properties of the membrane.

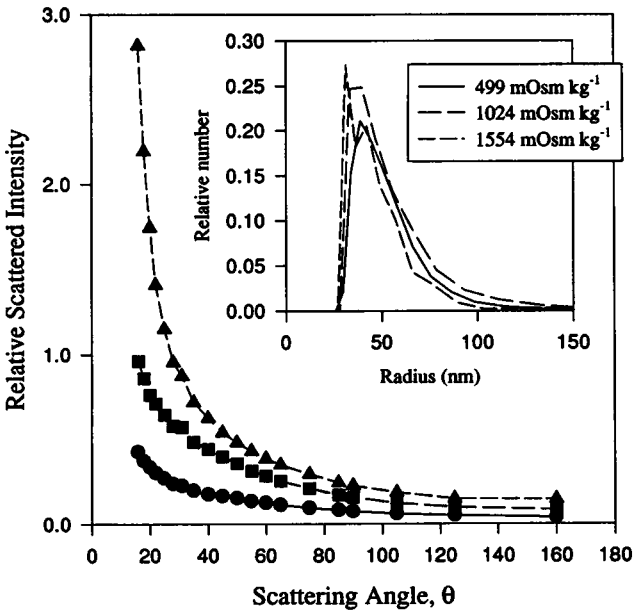

FIGURE 9 Relative scattered intensity as a function of scattering angle from vesicles prepared isotonically in varying concentrations of the osmolyte (NaCl). The scattered intensity increases as a function of osmolality. The inset shows the size distribution of vesicles in each sample and indicates that neither aggregation nor fusion is responsible for the changes in scattered intensity.

Although there is considerable literature dealing with the effects of solutes on bilayer properties, a clear understanding of the relationships among solutes, membrane hydration, and packing density is still lacking. Changes in packing density have been implicated by Yi and MacDonald (1973) to account for the abrupt scattering changes that take place at the gel-liquid crystal phase transition in dipalmitoylphosphatidylcholine. Different anionic osmolytes have been ranked according to the extent that they modify the phase properties of bilayers and were, therefore, thought to influence the packing arrangement of phospholipids (Sanderson et al., 1991). Lehtonen and Kinnunen (1995) have provided evidence that acyl chain packing density is the property through which osmolytes modulate the activity of phospholipase A_2 and cite numerous other references in support of their conclusions. In earlier work (Lehtonen and Kinnunen, 1994) they provided evidence indicating that changes in membrane volume and phospholipid packing densities could be attributed to hydration changes to the bilayer resulting from the addition of polyethylene glycol to the extravesicular medium. Rudolph et al. (1986) have shown that the spacing between headgroups and phase behavior can be significantly perturbed by the presence of solutes such as trehalose, proline, and betaine and attribute these perturbations to changes in hydration. Winterhalter (1996) has concluded that bending rigidity of the bilayer is basically governed by the extent of hydration. If hydration changes are present to the extent that they can affect the packing density and the bending rigidity, then presumably they could affect the optical properties as well. However, hydration could involve rearrangements of the headgroups of the phospholipid and leave the acyl chains relatively unaffected. Abuin et al. (1995) have suggested, from studies based on the analysis of fluorescence depolarization results from intrinsic membrane probes, that neither the presence of salt nor the osmotic imbalance modifies the hydrocarbon matrix of the bilayer. In this study we have treated the bilayer as a uniform structure with a single refractive index. With this simple approach, if the change in membrane refractive index indicated by Fig. 8 is entirely attributed to a change in the extent of hydration, then a simple volume-based calculation would estimate about 25% more bound water at maximum downshift as compared to the isotonic case. If the packing density of the acyl chain region is also reduced during hydration, then the reduction in refractive index could be achieved by adding less than 25% bound water. This percentage should be viewed, therefore, as an upper limit.

If the headgroup region of the bilayer is presumed to be the main region affected by hydration, then the resulting optical changes would be expected to occur predominantly in the headgroup region as well. With increasing hydration the refractive index of the headgroup region could become more closely matched to that of the medium. If a perfect match of the refractive indices of the headgroup region and the medium occurred, then the headgroup region would vanish optically and the membrane would exhibit an apparent thinning. Using Eqs. 1–8, it can be shown that an apparent reduction in t could lead to a significant reduction in the scattering intensity. Thus if the medium used for extrusion (the isotonic medium) were chosen to have a refractive index that closely approximates that of the headgroup region, optical changes in the headgroup region during osmotic upshift or downshift should largely be masked. To check this, DOPG vesicles were prepared in 1) 40% (~4 M) glycerol and 2) 37% (~4 M) betaine, both of which have a refractive index (at 589 nm) of 1.387. Higher concentrations than this made the extrusion procedure very slow and difficult. These preparations were then used as the starting point for a series of osmotic downshift experiments, the results of which are shown in Fig. 10. The media used for these downshift experiments contained the same glycerol (or betaine) concentration as the extrusion medium, but with lower sodium chloride concentrations to yield the final osmolality shifts shown on the diagram. Because the overall scattering intensities were significantly lower (due to the smaller value of m_1), these experiments were much more difficult and time-consuming to perform. Nevertheless, in the case of glycerol, osmotic downshifts in the extravesicular medium clearly lead to a small (~10% ± 2%) increase in the scattering intensity at low angles, a result that is consistent with the earlier theoretical prediction that assumed constant n_1 during swelling. The same experiment performed with betaine showed a small (~6% ± 5%) intensity decrease with increasing osmotic downshift, although the experimental error was somewhat larger in this

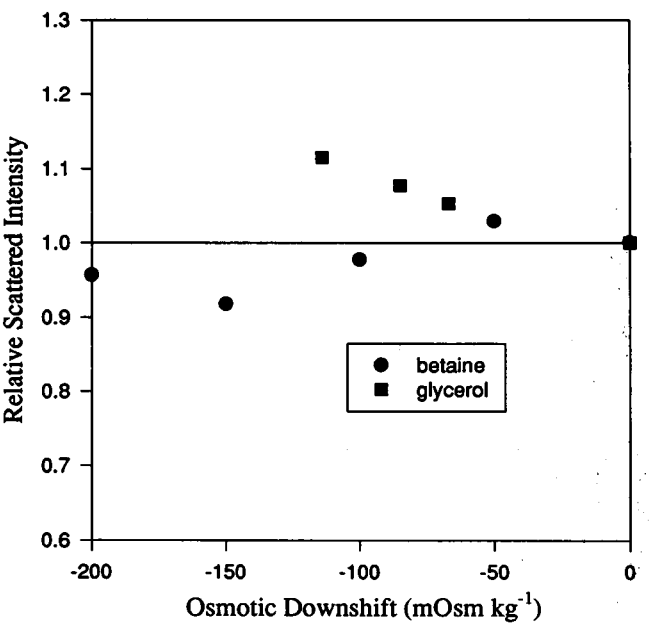

FIGURE 10 Relative scattered intensity as a function of osmotic downshift (due to varying the NaCl concentration) in media containing constant concentrations of glycerol and betaine. The scattered intensity showed only a small increase (in the case of glycerol) or slight decrease (in the case of betaine) rather than the large reduction in scattered intensity obtained in their absence (see Fig. 7).

case. In neither of these media did we observe the large reduction in scattered intensity with osmotic downshift that was observed earlier with the NaCl media (see Fig. 7).

In addition to altering the refractive index of the suspending medium, glycerol and glycine betaine could influence the behavior of this vesicle system by hydrogen bonding to polar functional groups within the phospholipid headgroup region or by penetrating the membrane, thereby influencing its refractive index. Both glycerol (Sanderson et al., 1991, and references cited therein) and betaine (Rudolf et al., 1986) are known to influence phospholipid phase behavior. Glycerol is membrane permeant, whereas betaine (Rudolf et al., 1986) is not. Because these compounds interact differently with the phospholipid bilayer, their effects on the scattering behavior of our vesicle system are likely to reflect these differences. However, because the large scattering changes observed previously are not seen when glycerol and betaine are present to optically mask the headgroup region, these studies provide further evidence that the scattering changes seen earlier can be attributed to changes in the membrane refractive index that arise due to modifications in the amount of headgroup hydration. This is not conclusive, however, because at the high osmolalities of glycerol or betaine, the membrane may be so dehydrated that the relatively small osmotic downshifts could lead to relatively small changes in hydration. Clearly, further experimental and modeling studies are required to confirm the relative roles of phospholipid packing and hydration in determining the total optical properties of the bilayer.

CONCLUSIONS

This study has shown that the phospholipid bilayer exhibits a significant change in refractive index in response to changing osmolalities of the solution environment. This optical change is believed to be primarily due to variations in the extent of bilayer hydration. It is expected that the headgroup region of the bilayer may experience shifts in packing density as water enters or leaves this region, and this may also lead to alterations in the packing density of the acyl chains. Analogous effects on the hydration and intramolecular or intermolecular packing of transmembrane helices may be anticipated for integral membrane proteins in membrane vesicles. Variations in the extent of hydration of membrane lipid and protein coupled with concomitant modifications in packing density could form the basis for mechanisms by which those membrane proteins involved in osmoregulation sense osmotic change in the cellular environment. However, some such proteins have been shown to sense changes in transmembrane osmolality gradient, but not in osmolality per se (e.g., Milner et al., 1988). Further studies designed to differentiate the effects of osmolality gradients from those of osmolality per se on the structures and interactions of membrane constituents will therefore be necessary to establish a basis for our understanding of those osmosensory mechanisms.

These studies have also shown that considerable caution must be exercised in the interpretation of either dynamic light-scattering data or static light-scattering data from vesicles in hypotonic or hypertonic media. In the hypotonic case both the refractive index of the bilayer and the refractive index of the lumen may differ significantly from their isotonic values, and these differences must be expressly incorporated into analyses leading to size distributions. Indeed, it is likely that treating the bilayer as a uniform structure with a single refractive index may be too simplistic for these conditions. We are attempting simulations using a three-layer model, in which the bilayer headgroups have a refractive index different from that of the acyl chain region. In the case of hypertonic media, the changing particle shape is an additional complication. A possible signature of nonsphericity in the vesicles might occur in the depolarized light-scattering modes, but we have not yet investigated this point.

APPENDIX A: ENERGETICS OF OSMOTICALLY STRESSED VESICLES

We describe below the expected size and shape changes induced in vesicles subjected to osmotic stress on the basis of a simplified but still realistic free energy. The important contributions to the free energy are from vesicle surface bending and stretching and from solute concentration gradients. This analysis was necessary for choosing, for the purpose of predicting light-scattering intensities, the most realistic models for vesicle shrinkage and swelling. It is demonstrated, for example, that the refractive index of the lumen equals the refractive index of the extravesicular medium at all osmotic upshifts. We will for convenience write all expressions relative to those for a spherical vesicle in isotonic conditions. The radius, surface area, and volume of this reference vesicle will be denoted by R_o, S_o, and V_o, respectively.

For the ellipsoidal vesicle curvature energy we take

$$E_c = \frac{1}{2} k_c \int dS(c_1 + c_2)^2 - 8\pi k_c, \qquad \text{(A1)}$$

(Deuling and Helfrich 1976), where the combination $c_1 + c_2$ is the mean curvature of the surface. In writing Eq. A1 we have made the reasonable assumption, based on the fact that only one type of phospholipid is present, that our vesicle bilayers are symmetrical and hence that there is no spontaneous curvature contribution. The bilayer bending rigidity k_c is thought to be typically about 1×10^{-19} J, although a recent measurement on DOPC by Niggemann et al. (1995) yielded $k_c \approx 0.3 \times 10^{-19}$ J. For the surface stretching contribution we use

$$E_s = \frac{1}{2} k_y t S_0 \left(\frac{S}{S_0} - 1 \right)^2, \qquad \text{(A2)}$$

where k_y is the membrane Young's modulus and t is the membrane thickness. The product $k_y t$ is the area compressibility for which recent literature gives the factor 2 range of 0.17–0.34 N/m (Hallett et al., 1993). Finally, we model the solvent/solute as an ideal solution and write its free energy contribution (in terms of internal energy E, entropy S, temperature T, and pressure P) as that of a perfect gas, $G_{sol} = E - TS + PV$, from which

$$G_{sol} = -Nk_B T \ln(V/V_o) + P(V - V_o), \qquad \text{(A3)}$$

where k_B is Boltzmann's constant and T is the temperature (Kelvin). The vesicle is assumed to be impervious to solute, so the number of particles N

in the vesicle lumen is fixed by the concentration of the medium in which the vesicles are prepared. For spheres of approximately 50-nm radius (number average) in 1500 mOsm/kg solution, $N \approx 4 \times 10^5$. The pressure P is the osmotic pressure external to the vesicle, and we will often write it below relative to the isotonic value, i.e., $p = P_{iso} + \Delta P_{ext}$, where $P_{iso} = Nk_BT/V_0$.

As written above, the free energy $G = E_c + E_s + G_{sol}$ is a function of the vesicle shape, surface area S, and volume V in addition to the controlling pressure P and temperature T. Assuming for the moment that fluctuations are negligible, the thermodynamic free energy $G = G(P,T)$ is to be understood as the minimum of G with respect to the shape, area, and volume variables. This minimization is discussed below, but first note that much of the qualitative behavior of the vesicles can be understood on the basis of the relative magnitude of the three contributions E_c, E_s, and G_{sol}. For the 50-nm radius (number average) vesicles used in this study, the ratio of the constants determining these contributions is $8\pi k_c : k_y t S_0 : Nk_BT \approx$ 1:10000:2000, although with a considerable range because of uncertainties in the membrane constants. Even so, we can conclude immediately that curvature plays a negligible role, with the exception of determining the shape of the vesicle under osmotic upshift conditions, where the shape is not determined by the other two terms.

Osmotic downshift

Influx of water causes vesicle swelling and the vesicle maintains its spherical shape. The curvature term $E_c = 0$ for a sphere, whereas the area $S = 4\pi R^2$ and volume $V = (4\pi/3)R^3$ are not independent. Minimization of G with respect to R gives

$$\Delta P_{ext} = -\frac{\Delta R}{R_0}\left(4k_y\frac{t}{R_0} + 3P_{iso}\right) \tag{A4}$$

in the limit that $\Delta R = R - R_0$ is small. The two terms on the right-hand side of Eq. A4 are the pressure differential across the membrane and the drop in the lumen pressure relative to the isotonic value, respectively. We can thus express the pressure differential as

$$P_{int} - P_{ext} = -\frac{\Delta P_{ext}}{(1 + (3/4)(P_{iso}R_0)/k_y t)} \tag{A5}$$

and note that the denominator in Eq. A5 lies in the range from ~1.5 to ~2.0 for our spheres of (intensity average) radius ≈ 70 nm. Thus the membrane, for our relatively small vesicles, is strong enough to maintain a considerable pressure gradient. By writing Eq. A5 in terms of concentrations, we obtain Eq. 10, which is necessary for calculating the light scattering.

Osmotic upshift

Water drainage from the lumen now collapses the vesicle to a nonspherical configuration of smaller volume. Jenkins (1977) has calculated the shapes for which the variation of E_c vanishes. The more recent work of Seifert et al. (1991) makes it clear that the shapes resembling a prolate ellipsoid of revolution are the minimum energy configurations, provided the volume has been reduced from its value for a sphere by less than about 35%. Because this is the regimen used here, we will not refer to any other shapes. Only a few more details of the variational curvature energy calculations are important in the following. First we should note that the (dimensionless) minimum $E_c/(8\pi k_c)$ is a function only of the dimensionless ratio V^2/S^3, and this single function of one variable simultaneously determines the volume and surface area dependence of the curvature contribution to the free energy. Second, if we write this function (i.e., minimum $E_c/(8\pi k_c)$) as $g_c(x)$, where $1 - x = 6\sqrt{\pi}V/S^{3/2}$ is the volume of the deformed vesicle relative to a sphere, then $g_c(x) = 2x + O(x^{3/2})$ for small x. Finally, the conclusion can be drawn from the numerical work of Jenkins (1977) or Seifert et al. (1991) that dg_c/dx remains close to 2 in the interval $0 < x <$ ~0.2 and then increases fairly dramatically to 3 at $x \approx 0.3$ and 4 at $x \approx$ 0.35, beyond which the prolate shape is no longer the minimum energy configuration.

To obtain the free energy $G(P,T)$ and the equilibrium vesicle area and volume, we must now minimize $G = 8\pi k_c g_c(x) + E_s + G_{sol}$ with respect to S and V separately. The result is the pair of equations

$$\begin{aligned} S &= S_0\left(1 - \left[\frac{12\pi k_c}{k_y t S}\right](1 - x)\frac{dg_c}{dx}\right) \\ V &= \frac{Nk_BT}{P}\left(1 + \left[\frac{8\pi k_c}{Nk_BT}\right](1 - x)\frac{dg_c}{dx}\right), \end{aligned} \tag{A6}$$

but because the dimensionless factors in [] above are on the order of 10^{-4} to 10^{-3}, we can use the very simple $S \approx S_0$, $V \approx Nk_BT/P$. This confirms the statement earlier that in the sense defined by Eq. A6, the curvature energy plays no role. There is a remaining very important point, namely the fact that the vesicle volume scales inversely as the external pressure implies that the internal and external solute concentrations remain identical. This, in turn, implies that the light scattering arises only from the vesicle shell (i.e., no contribution from the lumen). The final implication of this statement is that the Rayleigh-Gans-Debye treatment of the scattering becomes exact for thin-walled vesicles, as described in Appendix B.

Fluctuations

Because our vesicles are not large macroscopic objects, it is not obvious a priori that thermal fluctuations do not considerably modify the above results. We will not treat the general case but rather restrict ourselves to a discussion of the fluctuations at isotonic conditions. We further restrict ourselves to the largest amplitude shape distortions that correspond to the deformation of the sphere into an ellipsoid with principal semiaxes a, b, and c, with mean $(a + b + c)/3 = R$. Such a distortion can conveniently be parameterized as $a = R(1 + \delta\cos(\lambda))$, $b = R(1 + \delta\cos(\lambda - 2\pi/3))$, $c = R(1 + \delta\cos(\lambda + 2\pi/3))$ in terms of the small amplitude δ and the arbitrary phase λ that determine the relative magnitudes of a, b, and c. The minimum free energy is $G(P,T) = 0$, corresponding to a sphere of radius R_0. To quadratic order in δ and $\Delta R = R - R_0$, we have the excess:

$$G = \frac{48}{5}\pi k_c\delta^2 + \left[\frac{9}{2}Nk_BT + 2k_y t S_0\right]\left(\frac{\Delta R}{R_0}\right)^2. \tag{A7}$$

On setting these fluctuation terms separately to k_BT, we find a typical $\delta <$ 10% and $\Delta R/R_0 < 0.1\%$. Neither is significant for our analysis of the light scattering from these vesicles.

APPENDIX B: LIGHT SCATTERING FROM ELLIPSOIDAL SHELLS

This appendix describes the changes in scattering intensity that occur as a spherical vesicle changes its shape to an oblate ellipsoid of revolution under conditions of constant surface area but reduced volume, as discussed in Appendix A. Here also our experimental conditions are such that there is no scattering from the lumen. This considerably simplifies the treatment below and in a sense makes it exact. The known minimum curvature energy surface is not strictly ellipsoidal, and the actual shape can only be determined numerically (Jenkins, 1977; Seifert et al., 1991). It is not, therefore, convenient for an analytical treatment. But because our vesicles are small (~70 nm, intensity average radius) the differences in the shapes are not important. Indeed, a part of the analysis in this appendix is aimed at showing that the scattering from such small ellipsoids is adequately treated by the Guinier approximation and thus that no details other than radius of gyration are important.

We begin our discussion with a listing of some of the important formulae that describe an ellipsoid and then proceed to derive the intensity

of light scattered from a thin shell characterized by dielectric constant components $\epsilon_\perp$ and $\epsilon_\parallel$ perpendicular and parallel to the surface. Our framework is that of Rayleigh-Gans-Debye (RGD) but, for any thin-walled structure, this approach is exact in the sense of giving correctly the scattering amplitude to linear order in the shell thickness t. This point has been misunderstood in the literature (cf. Lange and Aragon, 1990; Hahn and Aragon, 1994) in part because of the frequently used technical trick of obtaining the scattering amplitude of a shell by the subtraction of the amplitude of two solid objects whose difference is the shell. The point to be made is that the RGD scattering amplitude from a solid object is not exact and the difference of two such expressions is not exact. Our approach treats the scattering from the shell directly and is not subject to this error. In particular, for each surface element we calculate exactly the dipole moment induced by an applied field, including the depolarization correction factor $1/\epsilon_\perp$ resulting from interactions with the dielectric surface in the immediate neighborhood. The effect of the dielectric in distant parts of the shell is negligible in the sense that it can only give rise to correction terms on the order of t^2.

Note that such a simplification is not possible for scattering from a solid object; in that case there is too much dielectric to allow a separation of depolarization effects into near and far regions. As an elementary illustration of the effects we are describing, consider the response of a thin spherical shell of isotropic dielectric ϵ to a uniform electric field. The polarization of the shell will be parallel to the field, applied in say a polar direction, only on the equator and at the poles. Elsewhere the polarization will be skewed away from the perpendicular to the surface because of the $1/\epsilon$ reduction of the perpendicular field component relative to the parallel. On the other hand, the polarization of solid spheres is everywhere parallel to the applied field, and if the shell were treated as the difference of two spheres the known polarization anisotropy could not be recovered.

We return now to ellipsoid formulae. For a prolate ellipsoid as shown in Fig. 11 we can define the eccentricity as

$$e = \sqrt{1 - \frac{b^2}{a^2}}, \tag{B1}$$

where a represents the long semiaxis and b the short semiaxis. From the geometry shown in Fig. 11 it can be seen that the surface area of the ellipsoid can be written

$$S = 2\pi\int \rho\sqrt{dz^2 + d\rho^2} = 2\pi ab\int d\theta \sin\theta\sqrt{1 - e^2\cos^2\theta},$$

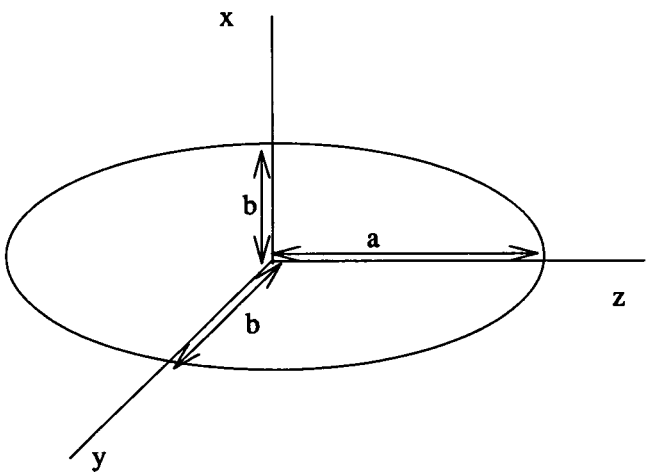

FIGURE 11 Figure B1: The coordinate system for ellipsoidal scatterers.

where the last expression follows using $z = a\cos\theta$, $\rho = b\sin\theta$. The final result is

$$S(e) = 2\pi ab\left(\frac{\sin^{-1} e}{e} + \sqrt{1 - e^2}\right) \tag{B2}$$

Because we require that the surface area not change as the lumen volume is reduced, we define

$$S(e) = S = 4\pi R_0^2 \tag{B3}$$

as in the text leading to Eq. 6. Then because $b(e) = a(e)\sqrt{(1 - e^2)}$, Eqs. B2 and B3 can be reverted to yield

$$a(e) = \sqrt{2}R_0\left(\sqrt{1 - e^2}\,\frac{\sin^{-1}(e)}{e} + 1 - e^2\right)^{-1/2}. \tag{B4}$$

The volume of the ellipsoid is

$$V(e) = \frac{4\pi}{3}(1 - e^2)a^3(e), \tag{B5}$$

but because it is the volume that is given by the osmotic upshift conditions, it is to be understood that Eqs. B4 and B5 will be reverted to determine $e = e(V)$. This can be done numerically by, say, Newton-Raphson iteration starting from the approximate ratio

$$\frac{b(e)}{a(e)} = 1 - \frac{1}{2}\sqrt{15x} + \frac{1.80x}{1 + 1.73\sqrt{x} - 0.80x}, \tag{B6}$$

where, as in the notation of Appendix A, $1 - x = 6\sqrt{\pi}V/S^{3/2}$ is the volume relative to a sphere. The first two terms in Eq. B6 are the exact Taylor series terms in the expansion of the ratio in $\sqrt{x}$, and the $O(x)$ term is a numerical approximation that makes Eq. B6 accurate to better than 0.002 for any $x < 1/2$, and an entirely adequate approximation for our purpose.

The mean radius of gyration of the ellipsoid is

$$R_g^2 = \frac{2\pi}{S}\int \rho(z^2 + \rho^2)\sqrt{dz^2 + d\rho^2}$$

$$= \pi\frac{b(e)a^3(e)}{S}\left[\left(\frac{5}{2} - 2e^2\right)\frac{\sin^{-1}e}{e} + \left(\frac{3}{2} - e^2\right)\sqrt{1 - e^2}\right]. \tag{B7}$$

The changes in radius of gyration with volume are shown in Fig. 12. Also shown for comparison purposes is the radius of gyration of the exact shapes described by Jenkins (1977) and Seifert et al. (1991). The impressive agreement between the two confirms our conclusion that, provided the Guinier approximation $I \propto 1 - Q^2R_g^2/3$ is valid, the exact vesicle shapes can be replaced by the much simpler ellipsoid model described here. As an aside we might comment that the somewhat larger differences seen between the two model radii of gyration for $x > \sim 0.3$ result from the fact that in this regime the exact shapes are of a very pronounced long cylindrical form.

The calculation of the light-scattering intensity from a thin shell, which for the moment we consider as placed in vacuum and characterized by $\epsilon_\perp$ and $\epsilon_\parallel$, follows in two steps. In the first instance one needs the **Q**-dependent polarizability tensor,

$$\underline{\alpha} = t/4\pi\int dS\,[(\epsilon_\parallel - 1)(\underline{\mathbf{1}} - \mathbf{nn}) + (1 - 1/\epsilon_\perp)\mathbf{nn}]$$

$$\cdot\exp(i\mathbf{Q}\cdot\mathbf{r}), \tag{B8}$$

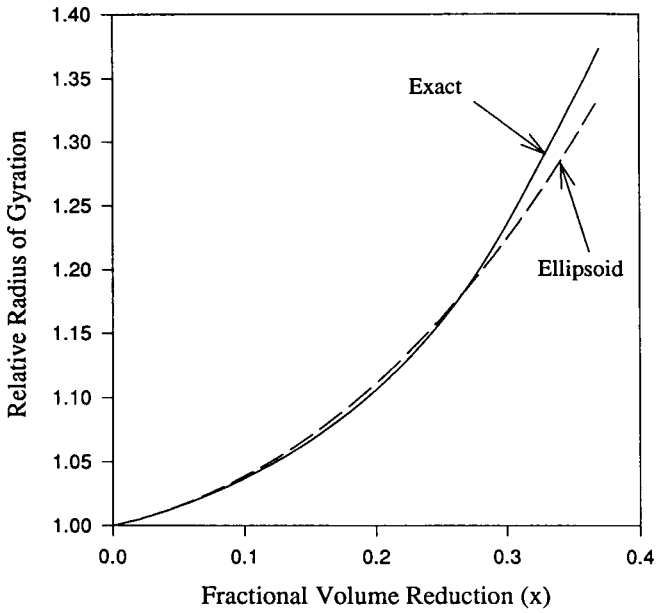

FIGURE 12 Figure B2: A comparison of the radius of gyration, relative to the initial sphere radius, of a prolate thin shell ellipsoid and the exact minimum energy shape as a function of the volume reduction factor x.

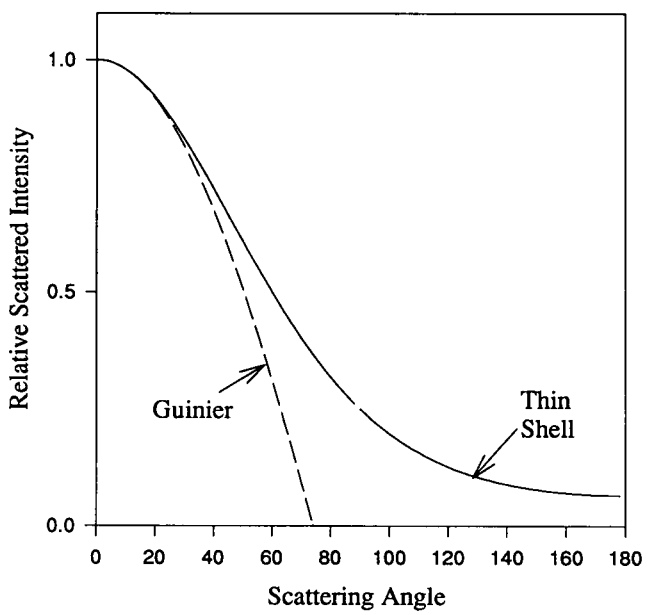

FIGURE 13 Figure B3: A comparison of scattering functions for a prolate thin shell ellipsoid at an osmotic upshift of 250 mOsm kg^{-1} (solid line) and the simpler Guiner function (dashed line), calculated using the same radius of gyration as the ellipsoid. With this upshift a spherical shell of radius 80 nm would become an ellipsoidal shell of axial ratio 2.3. The particle size is slight larger and the upshift is slightly more extreme than any actually used in the course of any of the experiments described above. These curves correspond, therefore, to a "worst case" situation. Even so, note that the two curves are essentially identical below 22° scattering angle.

which represents the polarization response of the shell to an applied electric field appropriately phased with the scattering vector $\mathbf{Q} = \mathbf{k}_f - \mathbf{k}_i$. In Eq. B8, $\mathbf{r}$ is the vector position of the surface element dS and $\mathbf{n}$ is the unit normal to the shell at that point. The two terms in [ ] are, respectively, the responses to an applied field parallel and perpendicular to the shell; they clearly show the inherent anisotropy due to depolarization, even if $\epsilon_\parallel = \epsilon_\perp$. Second, one needs to project the incident and scattered field polarization vectors λ_i and λ_f onto this tensor, then square the result and average over all possible orientations of the ellipsoid. That is, the final intensity is proportional to $\langle|\lambda_f \cdot \underline{\underline{\alpha}} \lambda_i|^2\rangle$, where $\langle\ \rangle$ denotes the orientation average.

To proceed with the details, note first that Eq. B8 can be rewritten as

$$\underline{\underline{\alpha}} = 1/S\int dS\{\alpha \underline{\underline{1}} + \beta/3(3\,\mathbf{nn} - \underline{\underline{1}})\}\exp(i\,\mathbf{Q}\cdot\mathbf{r}), \quad \text{(B9)}$$

where α and β are, respectively, the mean and anisotropic components of the polarizability. By explicitly comparing Eqs. B8 and B9, we find

$$\alpha = \frac{tS}{4\pi}\frac{2\epsilon_\parallel\epsilon_\perp - \epsilon_\perp - 1}{3\epsilon_\perp}$$
$$\beta = \frac{tS}{4\pi}\frac{2\epsilon_\perp - \epsilon_\parallel\epsilon_\perp - 1}{\epsilon_\perp}. \quad \text{(B10)}$$

On the assumption that the vesicle bilayer dielectric is intrinsically isotropic, so that $\epsilon_\perp = \epsilon_\parallel = \epsilon$, Eq. B10 reduces to

$$\alpha = \frac{tS}{4\pi}\frac{(\epsilon - 1)(2\epsilon + 1)}{3\epsilon} \quad \text{(isotropic case)}$$
$$\beta = -\frac{tS}{4\pi}\frac{(\epsilon - 1)^2}{\epsilon} \quad \text{(isotropic case).} \quad \text{(B11)}$$

If we now return to the real problem of a vesicle of one dielectric embedded in a medium of another, nearly equal dielectric, then the expression for α in Eq. B11 reduces further to

$$\alpha = \frac{tS}{2\pi}(m_1 - 1), \quad \text{(B12)}$$

where m_1 is the square root of the dielectric ratio as in Eqs. 1–7. The difference between the expressions for α in Eqs. B11 and B12 is small and cannot account for any of the scattering anomalies we observe. We have also shown that the contribution to the light-scattering intensity arising from nonzero β in Eq. B11 is at most a small fraction of 1% at all but 90° scattering, and even there only in the HH and HV components. Because of the small effect of β we will not discuss the full formula (B9) further here.

The contribution of the α or isotropic part of the polarizability tensor (B9) to the scattered light intensity is the simple expression (see Eq. 8)

$$I(Q) = \left(\frac{2\pi n_0}{\lambda}\right)^4 (\lambda_f\cdot\lambda_i)^2\alpha^2\left\langle\left|\frac{1}{S}\int dS\exp(i\mathbf{Q}\cdot\mathbf{r})\right|^2\right\rangle$$
$$\equiv \left(\frac{2\pi n_0}{\lambda}\right)^4 (\lambda_f\cdot\lambda_i)^2\langle P(Q)\rangle. \quad \text{(B13)}$$

The polarization vector scalar product $\lambda_f\cdot\lambda_i$ is unity for an experiment in the VV light-scattering mode and will not be considered further. Instead, in the rest of this appendix we discuss of the determination of the scattering factor $P(\mathbf{Q}) \equiv |A(\mathbf{Q})|^2$ with the amplitude

$$A(\mathbf{Q}) = \alpha/S\int dS\exp(i\,\mathbf{Q}\cdot\mathbf{r}). \quad \text{(B14)}$$

The coordinate system for evaluating the integral in Eq. B14 is as shown in Fig. 11, with the long axis of the ellipsoid along z and $\mathbf{Q}$ chosen in the x-z plane. Then $\mathbf{r}$ can be rescaled as in the integral leading to Eq. B2 by writing $z = a\cos\theta$, $x = b\sin\theta\cos\phi$, $y = b\sin\theta\sin\phi$. If we now take $\mathbf{Q}$ as inclined at an angle ψ to the z axis, $\mathbf{Q} = Q(\sin\psi\,\mathbf{i} + \cos\psi\,\mathbf{k})$, and the scalar product $\mathbf{Q}\cdot\mathbf{r}$ can be written $Q'(\cos\psi'\cos\theta + \sin\psi'\sin\theta\cos\phi)$, where

$$Q' = Qa\sqrt{1 - e^2\sin^2\psi}, \quad \cos\psi' = \frac{\cos\psi}{\sqrt{1 - e^2\sin^2\psi}}. \tag{B15}$$

Because of the form of the scalar product $\mathbf{Q}\cdot\mathbf{r}$ above, we can use the standard expansion

$$\exp(i\,\mathbf{Q}\cdot\mathbf{r}) = \Sigma_\ell(2\ell + 1)i^\ell j_\ell(Q')\{P_\ell(\cos\psi')P_\ell(\cos\theta) + 2\Sigma_m(\ell - m)!/(\ell + m)!P_\ell^m(\cos\psi')P_\ell^m(\cos\theta)\cos(m\phi)\} \tag{B16}$$

in the integrand in Eq. B14 to obtain

$$A(\mathbf{Q}) = \alpha\Sigma_\ell I_\ell j_{2\ell}(Q')P_{2\ell}(\cos\psi'),$$

$$I_\ell = I(e)_\ell = (4\ell + 1)(-1)^\ell 2\pi\frac{a(e)b(e)}{S}\int dz\sqrt{1 - e^2z^2}P_{2\ell}(z). \tag{B17}$$

The first two expansion constants I_ℓ are $I_0 = 1$ and

$$I_1 = \frac{5}{8}\left[1 + 3\left(1 - \frac{1}{e^2}\right)\frac{(\sin^{-1}e/e) - \sqrt{1 - e^2}}{(\sin^{-1}e/e) + \sqrt{1 - e^2}}\right], \tag{B18}$$

and the rest can be obtained by the recursion formula

$$I_{\ell+1} = \frac{(4\ell + 5)(2\ell - 1)}{(4\ell - 1)(\ell + 2)} \cdot\left[I_\ell - \frac{4\ell + 3}{4(\ell + 1)}\left[\frac{4\ell - 1}{(2\ell - 1)e^2}I_\ell + \frac{2\ell - 3}{4\ell - 3}I_{\ell-1}\right]\right]. \tag{B19}$$

The amplitude series in Eq. B17 is rapidly convergent, and one would rarely have to consider more than a few terms. Even in the extreme rod limit $e = 1$ the coefficients I_ℓ decay at large ℓ as ℓ^{-2}, as shown by the explicit formula

$$I(e = 1)_\ell = \frac{(-1)^{\ell+1}}{(2\ell - 1)}\frac{4\ell + 1}{\ell + 1}\left[\frac{\Gamma(\ell + (1/2))}{\Gamma(1/2)\Gamma(\ell + 1)}\right]^2. \tag{B20}$$

For nearly spherical vesicles the coefficients decay much more rapidly; one can show by expanding the square root in the integrand in Eq. B17 that

$$I_\ell = \frac{(-1)^{\ell+1}}{(2\ell - 1)}\frac{(2\ell)!^3}{\ell!^2(4\ell)!}e^{2\ell} + O(e^{2\ell+2}) \tag{B21}$$

for all ℓ in the limit $e \to 0$. This has the consequence that in the case of scattering from a sphere for which e is strictly 0, only $I_0 = 1$ survives and we get from Eq. B17 the standard result $P(\mathbf{Q}) = A(\mathbf{Q})^2 = \alpha^2 j_0(Qa)^2$, as given in Eq. 5.

The remaining step to the light-scattered intensity in the general case is that of averaging the square of $A(\mathbf{Q})$ as in Eq. B13. Although not possible analytically, it is an entirely straightforward numerical problem in which one simply interprets $\langle\ \rangle$ as $\frac{1}{2}\int d\psi\sin\psi$. Fig. 13 shows a comparison of $\langle P(\mathbf{Q})\rangle = \langle A(\mathbf{Q})^2\rangle$, with $A(\mathbf{Q})$ given by Eq. B17 and the general Guinier approximation

$$P(Q) = [2R_o^2 t_o(m_1 - 1)]^2(1 - Q^2R_g^2/3), \tag{B22}$$

with R_g^2 from Eq. B7. Clearly the two approaches are essentially identical at the scattering angles used in this study (<22°). We are confident, therefore, that the intensity changes that we observe cannot be explained by invoking shape deformation.

This research was supported by the Natural Sciences and Engineering Research Council of Canada.

REFERENCES

Abuin, E. B., A. M. Campos, E. A. Lissi, and E. A. Desalvo. 1995. Osmotic response of large unilamellar vesicles of phosphatidylcholine: factors determining the rate of the process and the properties of the shrunken vesicles. *J. Colloid Interface Sci.* 171:406–412.

Altendorf, K. H., and L. A. Staehelin. 1974. Orientation of membrane vesicles from *Escherichia coli* as detected by freeze-cleave electron microscopy. *J. Bacteriol.* 117:888–899.

Bangham, A. D., J. De Gier, and G. D. Greville. 1967. Osmotic properties and water permeability of phospholipid liquid crystals. *Chem. Phys. Lipids.* 1:225–246.

Bittman, R., and L. Blau. 1972. The phospholipid-cholesterol Interaction. Kinetics of water permeability in liposomes. *Biochemistry.* 11: 4831–4839.

Carruthers, A., and D. L. Melchior. 1983. Studies of the relationship between bilayer water permeability and bilayer physical state. *Biochemistry.* 22:5797–5807.

Csonka, L. N., and A. D. Hanson. 1991. Prokaryotic osmoregulation: genetics and physiology. *Annu. Rev. Microbiol.* 45:569–606.

Deamer, D. W., and J. Bramhall. 1986. Permeability of lipid bilayers to water and ionic solutes. *Chem. Phys. Lipids.* 40:167–188.

Deuling, H. J., and W. Helfrich. 1976. The curvature elasticity of fluid membranes: a catalogue of vesicle shapes. *J. Phys.* 37:1335–1345.

Engelbert, H.-P., and R. Lawaczeck. 1985. Isotopic light scattering of lipid vesicles. Water permeation and effect of α-tocopherol. *Chem. Phys. Lipids.* 38:365–379.

Ertel, A., A. G. Marangoni, J. Marsh. F. R. Hallett, and J. M. Wood. 1993. Mechanical properties of vesicles. I. Coordinated analysis of osmotic swelling and lysis. *Biophys. J.* 64:426–434.

Finkelstein, A. 1987. Water Movement Through Lipid Bilayer, Pores and Plasma Membranes. Wiley-Interscience, New York.

Freeman, M. H. 1990. Optics, 10th Ed. Butterworths, London.

Gregoriadis, A., editor. 1984. Liposome Technology. CRC Press, Boca Raton, FL.

Gregoriadis, A. 1995. Engineering Liposomes for drug delivery: progess and problems. *TIBTECH.* 13:527–537.

Grothe, S., R. L. Krogsrud, D. L. McClellan, J. L. Milner, and J. M. Wood. 1986. Proline transport and osmotic stress response in *Escherichia coli* K-12. *J. Bacteriol.* 166:253–259.

Hahn, D. K., and S. R. Aragon. 1994. MIE scattering from anisotropic thick spherical shells. *J. Chem. Phys.* 101:8409–8412.

Hallett, F. R., T. Craig, J. Marsh, and B. G. Nickel. 1989. Particle size analysis: number distributions by dynamic light scattering. *Can. J. Spectrosc.* 34:63–70.

Hallett, F. R., J. Marsh, B. G. Nickel, and J. M. Wood. 1993. Mechanical properties of vesicles. II. A model for osmotic swelling and lysis. *Biophys. J.* 64:435–442.

Hallett, F. R., J. Watton, and P. H. Krygsman. 1991. Vesicle sizing: number distributions by dynamic light scattering. *Biophys. J.* 59: 357–362.

Hallows, K. R., and P. A. Knauf. 1994. Principles of cell volume regulation. *In* Cellular and Molecular Physiology of Cell Volume Regulation. K. Strange, editor. CRC Press, Boca Raton.

Jansen, M., and A. Blume. 1995. A comparative study of diffusive and osmotic water permeation across bilayers composed of phospholipids with different head groups and fatty acyl chains. *Biophys. J.* 68: 997–1008.

Kaback, H. R. 1986. Active transport in *Escherichia coli*: passage to permease. *Annu. Rev. Biophys. Chem.* 15:279–319.

Kanchisa, M. I., and T. Y. Tsong. 1978. Cluster model of lipid phase transitions with application to passive permeation of molecules and structure relaxations in lipid bilayers. *J. Am. Chem. Soc.* 100:424–432.

Lange, B., and S. R. Aragon. 1990. Mie scattering from thin anisotropic spherical shells. *J. Chem. Phys.* 92:4643–4650.

Lawaczeck, R. 1979. On the permeability of water molecules across vesicular lipid bilayers. *J. Membr. Biol.* 51:1–33.

Lawaczeck, R. 1984. Water permeability through biological membranes by isotopic effects of fluorescence and light scattering. *Biophys. J.* 45: 491–494.

Lawaczeck, R. 1988. Defect structures in membranes: routes for the permeation of small molecules. *Ber. Bunsen-Ges. Phys. Chem.* 92: 961–963.

Lehtonen, J. Y. A., and P. K. J. Kinnunen. 1994. Changes in the lipid dynamics of liposomal membranes induced by poly(ethylene glycol): free volume alternations revealed by inter- and intramolecular excimer-forming phospholipid analogs. *Biophys. J.* 66:1981–1990.

Lehtonen, J. Y. A., and P. K. J. Kinnunen. 1995. Phospholipase A_2 as a mechanosensor. *Biophys. J.* 68:1888–1894.

Mayer, L. D., M. J. Hope, P. R. Cullis, and A. S. Janoff. 1985. Solute distributions and trapping efficiencies observed in freeze-thawed multilamellar vesicles. *Biochim. Biophys. Acta.* 817:193–196.

Milner, J. L., S. Grothe, and J. M. Wood. 1988. Proline Porter II is activated by a hyperosmotic shift in both whole cells and membrane vesicles of *Escherichia coli* K12. *J. Biol. Chem.* 263:14900–14905.

Mui, B. L.-S., P. R. Cullis, E. A. Evans, and T. D. Madden. 1993. Osmotic properties of large unilamellar vesicles prepared by extrusion. *Biophys. J.* 64:443–453.

Nayar, R., M. J. Hope, and P. R. Cullis. 1989. Generation of large unilamellar vesicles from long-chain saturated phosphatidylcholines by extrusion technique. *Biochim. Biophys. Acta.* 986:200–206.

Niggemann, G., M. Kummrow, and W. Helfrich. 1995. The bending rigidity of phosphatidylcholine bilayers: dependences on experimental method, sample cell sealing and temperature. *J. Phys. II.* 5:413–425.

Rand, R. P., and V. A. Parsegian. 1989. Hydration forces between phospholipid bilayers. *Biochim. Biophys. Acta.* 988:351–376.

Reeves, J. P., and R. M. Dowben. 1970. Water permeability of phospholipid vesicles. *J. Membr. Biol.* 3:123–141.

Rutkowski, C. A., L. M. Williams, T. H. Haines, and H. A. Cummins. 1991. The elasticity of synthetic phospholipid vesicles obtained by photon correlation spectroscopy. *Biochemistry.* 30:5688–5696.

Seifert, U., K. Berndl, and R. Lipowsky. 1991. Shape transformations of vesicles: phase diagram for spontaneous curvature and bilayer-coupling models. *Phys. Rev. A.* 44:1182–1202.

Sober, H. A. 1968. CRC Handbook of Biochemistry: Selected Data for Molecular Biology. The Chemical Rubber Co., Cleveland. E2–3.

Strawbridge, K., and F. R. Hallett. 1992. Polydisperse Mie theory applied to hollow latex spheres: an integrated light scattering study. *Can. J. Phys.* 70:401–406.

Strawbridge, K., and F. R. Hallett. 1994. Size distributions obtained from the inversion of $I(Q)$ using integrated light scattering spectroscopy. *Macromolecules.* 27:2283–2290.

Tanford, C. 1961. Physical Chemistry of Macromolecules. Wiley and Sons, New York.

Winterhalter, M. 1996. On the molecular origin of the bending elastic moduli. *Trends Colloids Interface Sci.* In press.

Wyatt, P. J. 1973. Differential light scattering techniques for microbiology. *In* Methods of Microbiology. J. R. Norris and D. W. Gibbons, editors. Academic Press, New York.

Yi, P. N., and R. C. MacDonald. 1973. Temperature dependence of optical properties of aqueous dispersions of phosphatidylcholine. *Chem. Phys. Lipids.* 11:114–134.

Yoshikawa, W., H. Akutsu, and Y. Kyogoku. 1983. Light scattering properties of osmotically active liposomes. *Biochim. Biophys. Acta.* 735:397–406.